Optimal parameters for the efficient microwave ablation of liver tumor from the 3D-IRCADb-01 database

NIKOLA BOŠKOVIĆ, BRANISLAV RADJENOVIC, MARIJA RADMILOVIĆ-RADJENOVIĆ*

Institute of Physics, University of Belgrade, Serbia.

Purpose: Microwave ablation is a minimally invasive thermal modality for cancer treatment with high survival and low recurrence rates. Despite the unquestionable benefits of microwave ablation, the interaction between the medical instruments and the tissue may cause damage to the healthy tissue around the tumor. Such damages can be removed by clarifying the conditions for their development. In addition to clinical methods, computer simulations have become very effective tools for optimizing microwave ablation performance. *Methods*: The study was focused on the determination of the optimal input power for complete microwave tumor ablation with an adequate safety margin avoiding injury to the surrounding healthy tissue. In three-dimensional simulations, the liver tumor model was based on a real tumor (1.74 cm × 2.40 cm × 1.43 cm) from the 3D-IRCADb-01 database. Calculations were performed for a 10-slot antenna proven to achieve a higher degree of ablation zone localization than a standard single-slot antenna. The temperature-dependent dielectric and thermal properties of healthy and tumoral liver tissue, blood perfusion, and water content were included in the model. *Results*: The obtained simulation results revealed that the proper choice of input power ensures that necrotic tissue is mainly located in the tumor with minimal damage to the surrounding healthy tissue. *Conclusions*: This study may represent a step forward in the planning of individual microwave ablation treatment for each patient.

Key words: microwave ablation, optimal conditions, tumoral tissue, necrotic tissue, three-dimensional simulation

1. Introduction

Liver cancer is one of the most common types of cancer worldwide and poses a significant health challenge because of its high mortality rate [1]–[5]. Treatment options for liver cancer may include surgery, liver transplantation, ablation therapy (such as radiofrequency or microwave ablation), embolization, chemotherapy, targeted therapy or immunotherapy. The choice of treatment depends on various factors such as tumor size and location, extent of liver damage, and overall health of the patient [6], [7].

The advantages of microwave ablation (MWA) in treating liver tumors include its ability to create larger ablation zones compared with other ablation techniques such as radiofrequency ablation, potentially improving treatment outcomes [8]–[10]. In addition, MWA may be more efficient in heating tissue, resulting in shorter procedure times. Although the effectiveness rate of MWA in removing small liver tumors is more than 85% for large tumors, completion rates are slightly lower [11], [12].

The mechanism underlying MWA is associated with an increase in temperature above the normal physiological threshold to kill cancer cells. A microwave antenna (MW) radiates an electromagnetic field, leading to frictional heating of water molecules in soft tissues [13]. The MW antenna design strongly affects the efficacy of MWA treatment [14]. Over the years, various antenna designs have been developed, including choke, cap-choke [15], floating sleeve [16], and water-cooled [17]. Recently developed compact multi-slot coaxial antennas ensure faster heating rates in the heating center and more localized heating distribution without damaging the surrounding healthy tissues than single-slot antennas [18].

The role of computational models in predicting medical treatment outcomes has significantly increased [19]–[23]. In most numerical studies, the degree of biological tissue destruction is determined by using the Arrhenius model [24]. Although three-dimensional (3D) simulations of radiofrequency ablation (RFA) exist [25], most simulations devoted to MWA are performed under the assumption of a homogeneous medium that reduces the problem from 3D to 2D, which often does not adequately represent reality [26]–[29].

In this study, simulations were performed using a three-dimensional simulation model [29]. A realistic model of the tumor was based on a real tumor denoted by 1.04 in the 3D-IRCADb-01 liver tumor database [30]. The primary goal of this study was to determine the optimal input power for complete tumor ablation with minimal damage to the surrounding healthy tissue. Estimation of the optimal power guarantees the best ratio of necrotic tissue to healthy tissue.

2. Numerical method

Modeling MWA as a multiphysics problem involves modeling multiple physical phenomena, such as electromagnetic wave propagation, heat transfer, and tissue damage, that occur during the procedure. The equation governing the electric field distribution through the tissue [29], [31] is as follows:

$$\nabla^2 \boldsymbol{E} - \mu_r k_0^2 \left(\varepsilon_r - \frac{j\sigma}{\omega \varepsilon_0} \right) \boldsymbol{E} = 0 \,, \qquad (1)$$

where ω is the angular frequency ω, $\boldsymbol{E}$ is the electric field vector, σ is the electrical conductivity of the tissue, and $k_0 = \omega/c_0$ is the vacuum propagation constant. ε_0, ε_r, and μ_r are the vacuum dielectric constant, relative permittivity, and permeability of the tissue, respectively.

The heat transfer is described by Pennes' bio-heat [29], [31]:

$$\rho c \frac{\partial T}{\partial t} = \nabla \times (k \nabla T) + \rho_b W_b c_b (T_b - T) + Q_{ext} + Q_m \,, \quad (2)$$

where t is the time. The parameters that characterize the tissue are density ρ, heat capacity c, and temperature T. Parameters associated with blood are density ρ_b, heat capacity c_b, temperature T_b, and perfusion rate W_b. In our calculations, the heat source from metabolism Q_m was neglected, whereas coupling with the electromagnetic field was included in the external heat source Q_{ext}.

During MWA, the tissue temperature increases leading to structural modifications of the treated tissue and causing changes in dielectric and thermal properties that affect the electromagnetic power distribution. The temperature dependence of the dielectric properties of the tissue is expressed by the following equations [29], [31]:

$$\varepsilon_r(T) = s_1 \left[1 - \frac{1}{1 + \exp(s_2 - s_3 T)} \right], \qquad (3)$$

$$\sigma(T) = r_1 \left[1 - \frac{1}{1 + \exp(r_2 - r_3 T)} \right], \qquad (4)$$

with the coefficients listed in [28]. It has been reported that the relative permittivity and conductivity of tumors are approximately by 24 and 11% higher than those of healthy tissue, respectively [29], [31]. The dielectric properties of both tumoral and healthy tissues decrease with increasing temperature because of water evaporation during MWA. Since liver tissue contains approximately 78% water, an increase in temperature above 100 °C may result in a decrease in tissue water content by approximately 20% by mass.

Tissue damage depends on both temperature and time according to the following Arrhenius form [29], [31]:

$$\Omega(t) = \int_0^t A \exp\left(-\frac{\Delta E}{RT} \right) \mathrm{d}t \,, \qquad (5)$$

where R and T are the gas constant and temperature, respectively. A is the frequency factor, while ΔE is the activation energy of the irreversible damage reaction. From the degree of tissue injury, the fraction of necrotic tissue θ_d can be calculated as follows [29], [31]:

$$\theta_d = 1 - \exp(-\Omega) \,. \qquad (6)$$

In this study, calculations were performed for a compact 10-slot antenna composed of several periodic elements, as shown in Fig. 1 [29]. Optimal ablation zones were achieved by adjusting the number of slots and the distance between them. Each periodic element complied with a slot and width of 0.6 mm and a spacing conductor of 0.8 mm between the two slots. Finely tuned impedance matching allows near-spherical ablation zones without damaging the surrounding healthy tissues. In contrast to the frequently used spherical tumor geometry, our simulation model is based on a real tumor labeled as 1.04 in the database 3D-IRCADb-01, which contains CT scans of several patients [30]. This tumor, which belonged to a female born in 1944 is relatively large (1.74 cm × 2.40 cm × 1.43 cm) with a volume
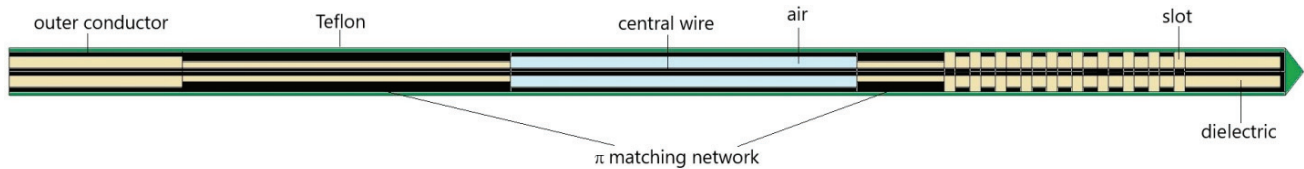
Fig. 1. Schematic representation of a 10-slot antenna with a finely tuned impedance π-matching network
to preserve surrounding healthy tissues. The distance between the two slots is 0.8 mm, while the width of the single slot is 0.6 mm

of 2.38 cm^3 and an irregular shape, as displayed in Fig. 2. One of the most critical steps in finite element calculations is meshing, which involves volume separation into many smaller elements. The mesh should be sufficiently fine to obtain accurate results, convergence and stability, but sufficiently coarse to avoid long computer time consumption. Our developed software [31] uses hybrid meshing with the combination of tetrahedrons, hexahedrons, pyramids and provides a highly accurate solution with much smaller number of elements compared to commercial softwares [19]–[23]. Unstructured meshing with only tetrahedrons would typically require millions of finite elements, and multiple refinement steps, to achieve sufficient quality and convergence. Most of the computational domain can be represented with regular geometries, which can easily be represented with structured meshing (hexahedrons) of superior quality, while complex geometry such as tumor can be represented with tetrahedrons and connected with the hexahedrons via a pyramidal layer. For these calculations, the mesh was composed of 78 469 tetrahedrons, 50 220 hexahedrons and 2233 pyramids.

To determine the optimal input power, numerical simulations were performed for tumor 1.04 from the database [30] exposed to a frequency of 2.45 GHz and input power in the range of 10–30 W. The parameters of the biological materials used in the numerical simulations are described in the literature [28], [29]. For the healthy liver, tumor, and blood samples, the density values (expressed in [kg/m^3]) were 1079, 1040, and 1060, respectively. The thermal conductivities in units W/m°C corresponding to healthy tissue, tumor tissue, and blood were 0.52, 0.57, and 0.5, respectively. Before treatment, the *tissue temperature* was assumed to be 37 °C.

3. Results

In Figure 3, the tumor (triangulated surface) and ablation zones (solid surfaces) are shown for an input power in the range of 10–30 W. The optimal value of the input power corresponded to total tumor ablation with minimal damage to healthy tissues. At an input power of
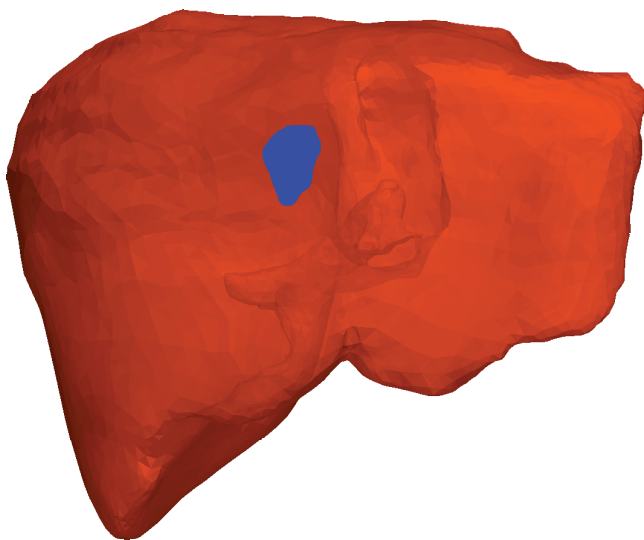

Fig. 2. Three-dimensional view of the liver (red solid surface) with the real position of tumor 1.04 taken from the database [30] (solid blue surface). Dimensions of tumor are
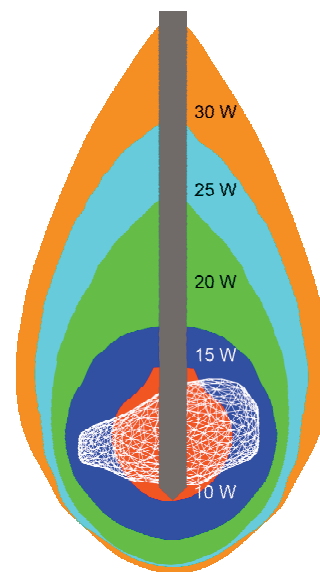(1.74 cm × 2.40 cm × 1.43 cm)

Fig. 3. Isocontours composed of the totally ablated region (solid surface) after 600 s of MWA of tumor 1.04 [30] (triangulated surface) for input power from 10 to 30 W

10 or 15 W, although the ablation zones were spherical, they did not ensure complete ablation of the tumor. With increasing the input power (25 or 30 W), ablation zones became more elongated, resulting in significant damage to healthy tissue around the tumor. Elongated shapes are undesirable ablation patterns that damage healthy tissues even if the ablation time is shorter. The ablation zone that best fit the necrotic tissue was achieved for an input power of 20 W, while the healthy tissue was preserved.

The fraction of necrosis around liver tumor 1.04 [30] (triangulated surface) during MWA at 20 W is shown in Fig. 4. The formed ablation zones are elongated with a greater length along the shaft of the antenna. The ablation zones are concentrated around the tip and slots of the antenna with two distinct heating zones [32]. The active heating zone appears within the tissue nearest to the antenna, where the intensity of energy is high and its absorption by the tissue is fast. The passive zone is far from the antenna, where the energy intensity is lower.

In Figure 5, the time evolution of the specific absorption rate (SAR), defined as the ratio of the absorbed heat power to tissue density, is presented [33]. The black lines represent tumor. The SAR increased along the axis and decreased after reaching a peak around the antenna slot. Although the maximal value of the SAR corresponds to the tumor area, the absorbed energy also invades the healthy surrounding tissue.

The time dependence of the temperature distribution around the tumor (triangulated surface) calculated for the estimated optimal power of 20 W is presented in Fig 6a. As the absorbed energy is converted into thermal energy, tissue temperature increases. In the vicinity of the antenna, the heat source is strong and the temperatures were higher. The temperature increased with ablation time and reached a maximum value inside the tumor region. The extent of heating is limited by the blood perfusion. Different cross sections of the temperature distribution at the end of the MWA at 600 s are illustrated in Fig. 6b.
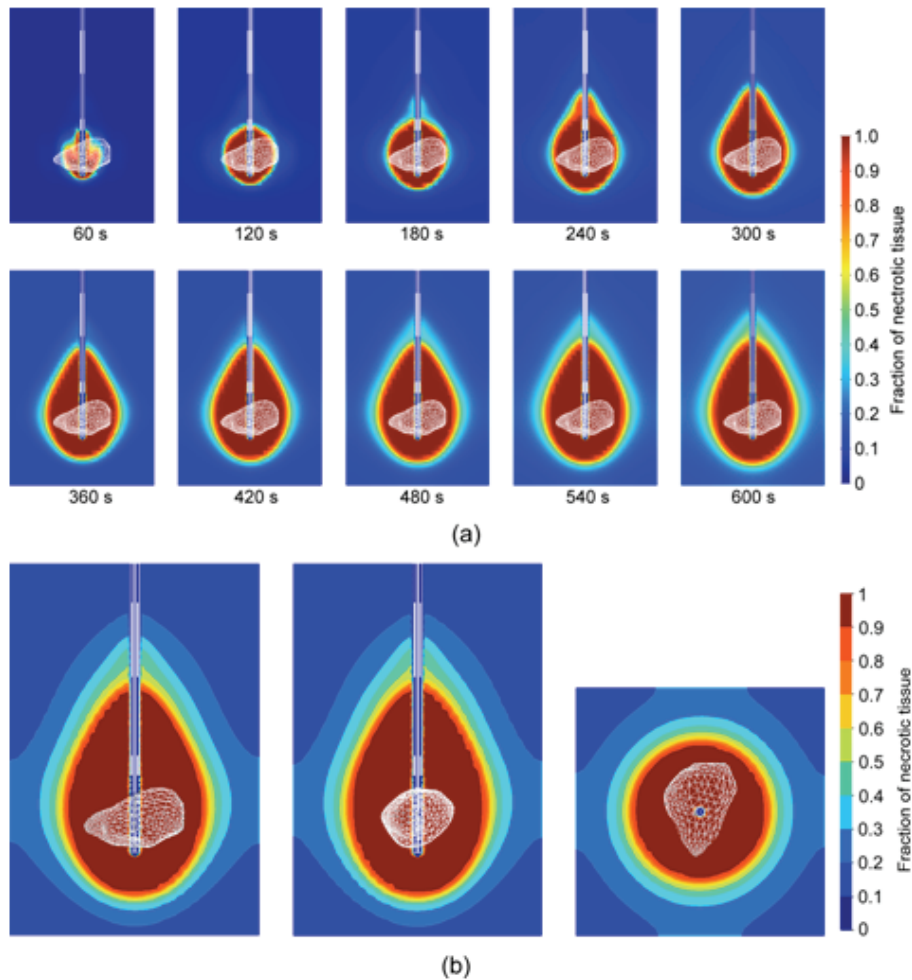

Fig. 4. (a) Time evolution of the fraction of necrosis from 60 s to 600 s, (b) fraction of necrotic tissue at different cross-sections at 600 s, around liver tumor 1.04 [30] (triangulated surface) during MWA at 2.45 GHz and input power of 20 W
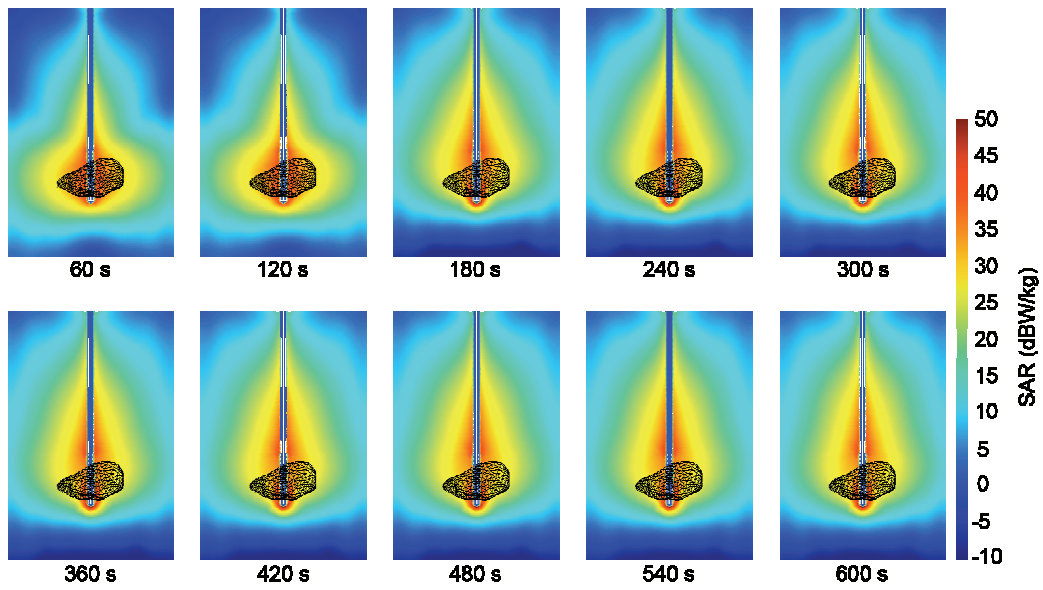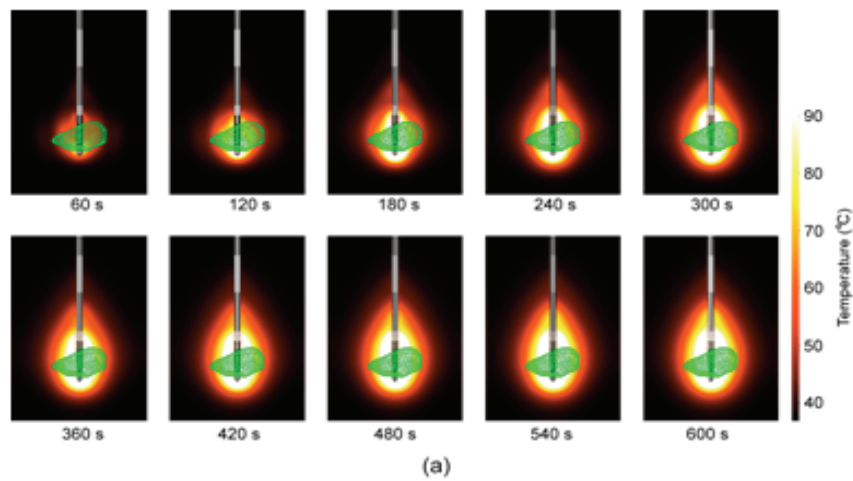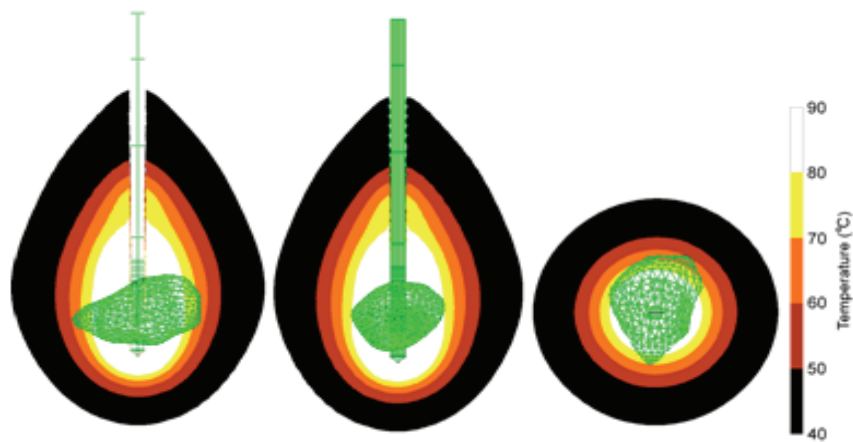
Fig. 5. (a) Time evolution of SAR distribution from 60 s to 600 s,
(b) SAR distribution at different cross-sections at 600 s, around liver tumor 1.04 [30]
(triangulated surface) during MWA at 2.45 GHz and input power of 20 W

Fig. 6. (a) The time evolution of temperature distribution from 60 s to 600 s,
(b) temperature distribution at different cross-sections at 600 s, around liver tumor 1.04 [30]
(triangulated surface) during MWA at 2.45 GHz and the input power of 20 W

4. Discussion

The size of the ablative zones depends on the amount of energy delivered from the microwave generator to the antenna. The fraction of damage increased as the ablation time increased. Even though the absorbed power density is high close to the antenna, the absorbed energy may also affect the healthy surrounding tissue. In our study, for an input power of 10 W, the ablation was small, located around the radiating slots. At 15 W, the ablation zone has a spherical shape. For higher input powers, ablation expansions are mostly focused in the longitudinal direction around the probe. The estimated optimal value of the input power of 20 W ensures complete tumor necrosis and sufficient safety margins. Ablation time decreased with increasing input power. However, even if the ablation time is shorter, higher input power values may result in the formation of elongated undesirable ablation zones, causing significant damage to healthy tissue around the tumor. Furthermore, delivery of high-power, short-duration ablation is not commonly used because of the increased risk of steam pop and thrombus formation [34].

The time evolution of the ablation shows that up to 120 s, the ablation remains highly spherical, after which it grows and elongates. In addition, the high-intensity SAR zones follow the ablation shape. Any tissue in the zone with a SAR of approximately 25 dBW/kg or more can be considered ablated. The temperature also increases with increasing ablation time and reaches a maximum value near the microwave antenna slots. Any tissue within the zone with a temperature above 60 °C is instantly ablated. The tissue inside the zone above 50 °C would typically be ablated after approximately 10 min, whereas prolonged exposure to temperatures above 42 °C can also cause irreversible tissue damage. The distribution of high temperature with time follows the form of necrosis. The entire tumor is located within the zone with a temperature of 60 °C and above, ensuring that MWA is successful.

In contrast to our simulation model, the 3D model of MWA implemented in the commercial ANSYS software includes parts of liver tissue, bones, skin and fat [23]. However, it does not include any tumor that affects the accuracy of the calculations because of different material parameters corresponding to tumoral and healthy tissue [23]. In addition, the duration of the simulation presented in [23] ranges between 15 and 20 days, whereas our simulations usually last around 100 minutes. Our 3D FEM simulation results obtained for a real tumor provide a much more accurate representation of the MWA process compared with simplified tumor geometry and 2D-axial symmetric simulations [26], [27]. Significant differences between results obtained using the 2D axisymmetric FEM model of the MWA and experimental results clearly indicate the importance of performing full 3D simulations [26]. When a 1-slot antenna is used [27], the tail of the so-called "comet-shaped" ablation zones obtained for sphere-like tumors unavoidably damages the healthy tissue along the shaft of the antenna as opposed to minimal surrounding tissue damage obtained in our results. Regarding antenna design, our results agree well with the 3D simulation results presented in [28], revealing that a 10-slot antenna offers higher heating efficiency of tissue and more near-spherical ablation zones than a 1-slot antenna.

Determining the optimal ratio of necrotic tissue to healthy tissue is important for improving MWA treatment to remove the maximal part of the tumor while preserving healthy surrounding tissue. Although a multi-slot coaxial antenna produces a more localized heating pattern for spherical tumors; for realistic tumor shapes, the ablation zones are usually elongated. In some cases, to treat larger tumors, two or three antenna systems are recommended.

5. Conclusions

In this study, we determined the optimal input power for efficient and safe microwave liver tumor ablation. For this purpose, full three-dimensional simulations based on a finite element method have been developed and tested [28], [30]. Calculations were performed for a model of a real liver tumor denoted by 1.04 in the database 3D-ICRADb-01 (3D-IRCADb) [29] exposed to radiation from a 10-slot antenna operating at a frequency of 2.45 GHz. Parameters characterizing healthy and tumoral tissues are included in the model. Since blood flow acts as cooling fluid, if not taken into account, the ablation estimation can be severely wrong. We assumed that there is no perfusion in necrotic tissue, hence blood perfusion increases with temperature until tissue necrosis, when it becomes zero. Since ablation processes follow the Arrhenius model, we used it to estimate tissue damage as a function of time.

The optimal value of the input power of 20 W was estimated so that the whole tumor was completely ablated with minimal damage to the healthy tissue. The presented results clearly show the importance of three-dimensional modeling in determining the optimal conditions MWA which may be incorporated into medical procedure planning for each tumor. Recent

advancements in simulation models of tissue damage may play a crucial role in the development of medical devices and the improvement of surgical therapeutic procedures.

Acknowledgements

References

[1] ANANTHAKRISHNAN A., GOGINENI V., SAEIAN K., *Epidemiology of Primary and Secondary Liver Cancers*, Semin. Intervent. Radiol., 2006, 23 (1), 47–63.

[2] BALOGH J., VICTOR D., ASHAM E.H., BURROUGHS S.G., BOKTOUR M., SAHARIA A., LI X., GHOBRIAL R.M., MONSOUR H.P. Jr., *Hepatocellular carcinoma: A review*, J. Hepatocell. Carcinoma, 2016, 3, 41–53.

[3] VILLANUEVA A., *Hepatocellular Carcinoma*, N. Engl. J. Med., 2019, 380, 1450–1462.

[4] LINN Y.L., CHEE M.Y., KOH Y.X., TEO J.Y., CHEOW P.C., CHOW P.K.H., CHAN C.Y., CHUNG A.Y.F., OOI L.L.P.J., GOH B.K.P., *Actual 10-year survivors and 10-year recurrence free survivors after primary liver resection for hepatocellular carcinoma in the 21st century: a single institution contemporary experience*, J. Surg. Oncol., 2021, 123 (1), 214–221.

[5] CHEN J.G., ZHU J., ZHANG Y.H., CHEN Y.S., DING L.L., CHEN H.Z., SHEN A.G., WANG G.R., *Liver Cancer Survival: A Real World Observation of 45 Years with 32,556 Cases*, Journal of Hepatocellular Carcinoma, 2021, 8, 1023–1034.

[6] LI Y., ZHANG R., XU Z., WANG Z., *Advances in Nanoliposomes for the Diagnosis and Treatment of Liver Cancer*, Int. J. Nanomedicine, 2022, 17, 909–925.

[7] KOULOURIS A., TSAGKARIS C., SPYROU V., PAPPA E., TROULLINOU A., NIKOLAOU M., *Hepatocellular Carcinoma: An Overview of the Changing Landscape of Treatment Options*, J. Hepatocell. Carcinom, 2021, 8, 387–401.

[8] XU X.L., LIU X.D., LIANG M., LUO B.M., *Radiofrequency ablation versus hepatic resection for small hepatocellular carcinoma: systematic review of randomized controlled trials with meta-analysis and trial sequential analysis*, Radiology, 2018, 287 (2), 461–472.

[9] GLASSBERG M.B., GHOSH S., CLYMER J.W., WRIGHT G.W.J., FERKO N., AMARAL J.F., *Microwave ablation compared with hepatic resection for the treatment of hepatocellular carcinoma and liver metastases: A systematic review and meta-analysis*, World J. Surg. Oncol., 2019, 17 (1), 98.

[10] REIG M., FORNER A., RIMOLA J., FERRER-FÀBREGA J., BURREL M., GARCIA-CRIADO Á., KELLEY R.K., GALLE P.R., MAZZAFERRO V., SALEM R., SANGRO B., SINGAL A.G., VOGEL A., FUSTER J., AYUSO C., BRUIX J., *BCLC strategy for prognosis prediction and treatment recommendation: The 2022 update*, J. Hepatol., 2022, 76 (3), 681–683.

[11] XU H., ZHANG Q., TAN Y.L., ZHANG Y., WEI J.Z., WANG L.L., XIE B., *Efficacy of microwave ablation and entecavir as a combination treatment for primary liver cancer and their effects on hepatitis B virus and liver function*, All Life, 2020, 13 (1), 524–531.

[12] HUMPHREY S., NEWCOMER J.B., RAISSI D., GABRIEL G., *Percutaneous microwave ablation for early-stage intrahepatic cholangiocarcinoma: A single-institutional cohort*, J. Clin. Imaging Sci., 2024, 13, 4.

[13] CURTO S., TAJ-ELDIN M., FAIRCHILD D., PRAKASH P., *Microwave ablation at 915 MHz vs 2.45 GHz: A theoretical and experimental investigation*, Med. Phys., 2015, 42 (11), 6152–6161.

[14] KARAMPATZAKIS A., KÜHN S., TSANIDIS G., NEUFELD E., SAMARAS T., KUSTER N., *Antenna design and tissue parameters considerations for an improved modelling of microwave ablation in the liver*, Phys. Med. Biol., 2013, 58 (10), 3191–3206.

[15] PRAKASH P., CONVERSE M.C., WEBSTER J.G., MAHVI D.M., *An optimal sliding choke antenna for hepatic microwave ablation*, IEEE Trans. Bio-Med. Eng., 2009, 56 (10), 2470–2476.

[16] YANG D., BERTRAM J.M., CONVERSE M.C., O'ROURKE A.P., WEBSTER J.G., HAGNESS S.C., WILL J.A., MAHVI D.M., *A floating sleeve antenna yields localized hepatic microwave ablation*, IEEE Trans. Bio-Med. Eng., 2006, 53 (5), 533–537.

[17] SUN Y.Y., CHENG Z.G., DONG L., ZHANG G.M., WANG Y., LIANG P., *Comparison of temperature curve and ablation zone between 915-and 2450 MHz cooled-shaft microwave antenna: Results in ex vivo porcine livers*, Eur. J. Radiol., 2012, 81 (3), 553–557.

[18] GE M., JIANG H., HUANG X., ZHOU Y., ZHI D., ZHAO G., CHEN Y., WANG L., QIU B., *A multi-slot coaxial microwave antenna for liver tumor ablation*, Phys. Med. Biol., 2018, 63 (17), 175011.

[19] WANG Q., YAN H., GUO M., MENG L., LONG Z., LONG Y., YANG H., *Three-dimensional finite element analysis of a novel interzygapophyseal fusion device for lower cervical spine*, Acta Bioeng. Biomech., 2022, 24 (2), 187–193.

[20] LIU P., WAN J., LIU W., ZHAO Y., YAN S., JIANG W., LIU H., *Numerical analysis of the effects of canal wall-up and canal wall-down mastoidectomy on the sound transmission characteristics of human ears*, Acta of Bioengineering and Biomechanics, 2023, 25 (2), 132–145.

[21] SU P., YANG Y., ZHANG L., HUANG L., *Biomechanical simulation of needle insertion into cornea based on distortion energy failure criterion*, Acta Bioeng. Biomech., 2016, 18 (1), 65–75.

[22] SERVIN F., COLLINS J.A., HEISELMAN J.S., FREDERICK-DYER K.C., PLANZ V.B., GEEVARGHESE S.K., BROWN D.B., JARNAGIN W.R., MIGA M.I., *Simulation of Image-Guided Microwave Ablation Therapy Using a Digital Twin Computational Model*, IEEE Open Journal of Engineering in Medicine and Biology, 2024, 5, 107–124.

[23] GORMAN J., TAN W., ABRAHAM J., *Numerical Simulation of Microwave Ablation in the Human Liver*, Processes, 2022, 10 (2), 361.

[24] QIN Z., BALASUBRAMANIAN S.K., WOLKERS W.F., PEARCE J.A., BISCHOF J.C., *Correlated parameter fit of arrhenius model for thermal denaturation of proteins and cells*, Ann. Biomed. Eng., 2014, 42 (12), 2392–2404.

[25] SHEU T.W., CHOU C.W., TSAI S.F., LIANG P.C., *Three-dimensional analysis for radio-frequency ablation of liver tumor with blood perfusion effect*, Computer Methods in Biomechanics and Biomedical Engineering, 2005, 8 (4), 229–240.

[26] ORTEGA-PALACIOS R., TRUJILLO-ROMERO C.J., CEPEDA-RUBIO M.F.J., LEIJA L., VERA HERNÁNDEZ A., *Heat Transfer Study in Breast Tumor Phantom during Microwave Ablation: Modeling and Experimental Results for Three Different Antennas*, Electronics, 2020, 9 (3), 535.

[27] Selmi M., Bin Dukhyil A.A., Belmabrouk H., *Numerical Analysis of Human Cancer Therapy Using Microwave Ablation*, Appl. Sci., 2020, 10 (1), 211.

[28] Tehrani M.H.H., Soltani M., Kashkooli F.M., Raahemifar K., *Use of microwave ablation for thermal treatment of solid tumors with different shapes and sizes – A computational approach*, PLoS ONE, 2020, 15 (6), e0233219.

[29] Radmilović-Radjenović M., Bošković N., Sabo M., Radjenović B., *An Analysis of Microwave Ablation Parameters for Treatment of Liver Tumors from the 3D-IRCADb-01 Database*, Biomedicines, 2022, 10 (7), 1569.

[30] 3D-IRCADb database, https://www.ircad.fr/research/3dircadb/ [Accessed: 25 January 2024].

[31] Bošković N., Radmilović-Radjenović M., Radjenović B., *Finite Element Analysis of Microwave Tumor Ablation Based on Open-Source Software Components*, Mathematics, 2023, 11 (12), 2654.

[32] Radmilović-Radjenović M., Radjenović D., Radjenović B., *Finite element analysis of the effect of microwave ablation on the liver, lung, kidney, and bone malignant tissues*, Europhys. Lett., 2021, 136, 1363500.

[33] Miaskowski A., Gas P., *Numerical Estimation of SAR and Temperature Distributions inside Differently Shaped Female Breast Tumors during Radio-Frequency Ablation*, Materials, 2023, 16 (1), 223.

[34] Mercado Montoya M., Gomez Bustamante T., Berjano E., Mickelsen S.R., Daniels J.D., Hernandez Arango P., Schieber J., Kulstad E., *Proactive esophageal cooling protects against thermal insults during high-power short-duration radiofrequency cardiac ablation*, International Journal of Hyperthermia, 2022, 39 (1), 1202–1212.